

See discussions, stats, and author profiles for this publication at: <https://www.researchgate.net/publication/265467551>

Characterization and Dynamic Properties for the Solid Inclusion Complexes of β -Cyclodextrin and Perfluorobutyric Acid

ARTICLE in THE JOURNAL OF PHYSICAL CHEMISTRY C · JUNE 2014

Impact Factor: 4.77 · DOI: 10.1021/jp502325e

CITATIONS

3

READS

43

4 AUTHORS, INCLUDING:



[Abdalla Hamisi Karoyo](#)

University of Saskatchewan

8 PUBLICATIONS 48 CITATIONS

SEE PROFILE



[Paul S Sidhu](#)

University of Lethbridge

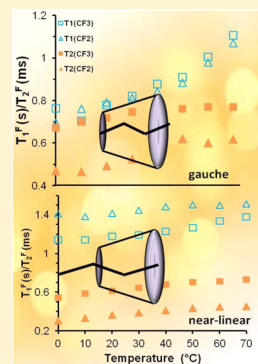
16 PUBLICATIONS 108 CITATIONS

SEE PROFILE

Characterization and Dynamic Properties for the Solid Inclusion Complexes of β -Cyclodextrin and Perfluorobutyric AcidAbdalla H. Karoyo,[†] Paul Sidhu,[‡] Lee D. Wilson,^{*,†} and Paul Hazendonk^{*,‡}[†]Department of Chemistry, University of Saskatchewan, Saskatoon, Saskatchewan S7N 5C9, Canada[‡]Department of Chemistry and Biochemistry, University of Lethbridge, Lethbridge, Alberta T1K 3M4, Canada

S Supporting Information

ABSTRACT: The structural characterization of solid- and solution-state inclusion complexes (ICs) of β -cyclodextrin (β -CD; host) with perfluorobutyric acid (PFBA; guest) is presented in this study. Complexes in the solid state were prepared at various host/guest mole ratios (i.e., 1:1 and 2:1) using a modified dissolution method. Thermal analyses and multinuclear ^{13}C NMR methods employing direct polarization (DP) and cross-polarization (CP) techniques with magic angle spinning (MAS) and high-power $^1\text{H}/^{19}\text{F}$ decoupling were used to characterize the solid-state host–guest complexes. Unequivocal evidence of the formation of β -CD/PFBA inclusion compounds was provided using $^{19}\text{F} \rightarrow ^{13}\text{C}$ CP/MAS NMR results. Powder X-ray diffraction reveals that PFBA forms a “cage-type” structure with β -CD, in which the guest adopts *gauche* and near-linear conformations in the 1:1 and 2:1 complexes, respectively, according to Fourier transform infrared spectroscopy results. Interpretation of the NMR splitting patterns of PFBA spectrum in solution reveals that PFBA undergoes fast rotation of the CF_3 group on a 3-fold axis, while the remainder of the chain experiences a significant C–C bond rotation; hence, it is not locked in a particular rotamer configuration. The distribution of the rotational and axial motions in the β -CD/PFBA complexes in the solid state as revealed by NMR relaxation dynamic studies is a function of the host/guest mole ratios and is determined by the binding geometry of the guest.



1. INTRODUCTION

There is vast research interest in perfluorinated compounds (PFCs) because they represent a new class of persistent organic pollutants (POPs) found in Canada and globally. PFCs are a class of fluorine-containing compounds that are surface active and generally resistant to chemical and thermal degradation.¹ They are used in many applications such as surfactants, adhesives, cosmetics, pesticides, and firefighting foams and powders.^{1,2} Several studies have documented the occurrence of several main classes of PFCs in the environment; namely, perfluoroalkyl carboxylic acids (PFCAs, e.g., PFOA) and perfluoroalkyl sulfonates (PFSSs, e.g., PFOS).^{3–8} PFCAs ($\text{CF}_3(\text{CF})_n\text{CO}_2\text{H}$) and PFSSs ($\text{CF}_3(\text{CF})_n\text{SO}_3\text{H}$) have been detected in soil and sediments, groundwater, fish and animal tissues, sewage effluent, and other matrices.^{7,8} In general, PFCAs with alkyl chains that are 4–10 carbons long were reported to be the most dominant species detected in landfill leachates in the Americas.^{9,10} The distribution of PFCs in water, air, and sediment was found to depend on their physicochemical properties.⁶ Therefore, the distribution of such compounds onto solid surfaces varies according to differences in properties such as pK_a , solubility, and vapor pressure. These properties are directly related to the alkyl chain length and the structure of the headgroup.¹¹ On the basis of known physical properties (cf. Table 1), PFOS is essentially nonvolatile and more soluble than PFOA and displays a strong tendency to exist in aqueous solution. PFBA is much more mobile than PFOA and PFOS because of its greater water solubility and

shorter alkyl chain length. Therefore, PFBA can favorably reside in ground and surface water environments. The short-chain PFCAs are primarily detected as dissolved species, whereas long-chain PFCAs are mostly adsorbed onto solid interfaces, such as suspended solids and sediments. The structures and physicochemical properties of several PFCs are given in Table 1.

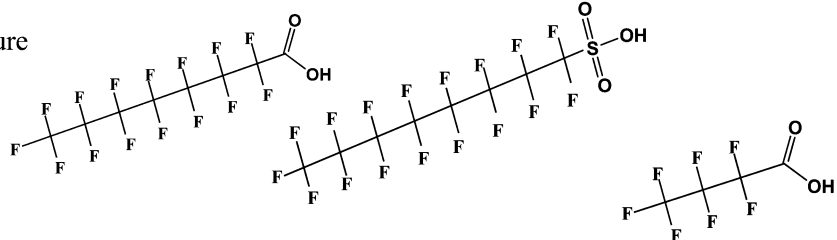
We previously reported¹² the formation of solid inclusion complexes between β -CD and PFOA. As well, similar complexes were formed using the conjugate base of PFOA (i.e., sodium perfluorooctanoate; SPFO).¹³ Such complexes were generally characterized using a variety of techniques including NMR and Fourier transform infrared (FT-IR) spectroscopy, thermal analyses, and powder X-ray diffraction (PXRD). Understanding the structure of PFCs and their complexes with CDs¹⁴ is crucial because it helps develop better host systems for immobilizing these compounds in the environment. PFOA (and SPFO) were previously shown to form both 1:1 and 2:1 ICs with β -CD with variable binding configurations. Ellis et al.⁵ and other researchers^{15,16} have demonstrated that changes in the chain length of a perfluorocarbon compound correlates with changes in its conformation and physicochemical properties (e.g., critical micelle concentration, pK_a , melting and boiling points,

Received: March 6, 2014

Revised: June 24, 2014

Published: June 24, 2014

Table 1. Physicochemical Properties of Selected Perfluorocarbon Compounds^{a,16,20–24}

	PFOA	PFOS	PFBA
Molecular Formula	C ₈ HF ₁₅ O ₂	C ₈ HF ₁₇ O ₃ S	C ₄ HF ₇ O ₂
and Structure			
Molecular weight (g/mol)	414	500	214
Solubility (g/L, 25°C)	0.34	0.57	High Solubility
Melting Point (°C)	45–55	>400	-17.5
Boiling Point (°C)	188	133	120
pK _a	2.5	0.14	0.08–0.4
CMC (mmol/L)	8.5–10	2.0	No data
Vapor pressure (mmHg, 25°C)	0.017	2.48×10 ⁻⁶	10

^aNote that the conformation and stereochemistry of the PFCs are not accurately depicted.

solubility, and viscosity). Many of the aforementioned physical properties play a vital role in the environmental fate and distribution of PFCs in the environment. The conformational preference of a perfluorocarbon chain in its native state influences the way PFCs interact with CDs to form host–guest complexes. Bunn et al.¹⁷ explained that the helical conformation adopted by medium and long perfluoroalkyl chains results in a significant increase (~3 units) in pK_a from PFBA (0.40) and trifluoroacetic acid (TFA; 0.23)¹⁸ to PFOA (2.5–3.8).¹⁶ In general, the chain conformation of perfluorocarbon compounds is best described as being fully zigzag (or *trans*) for alkyl chain lengths ≤8 carbons, a mixture of zigzag and helical for alkyl chain lengths 8–12 carbons, and fully helical (*gauche*) for alkyl chain lengths >12 carbon atoms. Thus, the general trend in the geometry of perfluoroalkyl chains is the progression of a planar zigzag to helical geometry with increasing chain length. Thus, the physicochemical properties in Table 1 vary with the perfluoroalkyl chain length.

We report the structural characterization of the complexes formed between PFBA and β-CD. We also report on the dynamic properties of PFBA in its pure form in solution and its complexed form with β-CD in the solid state. PFBA represents a model guest compound possessing a relatively short PFC chain (C4). The study of the formation of complexes of PFBA with β-CD will provide an improved understanding of the structure of hydrophilic PFCs with relatively short carbon chains. The complexes were prepared at the 1:1 and 2:1 host/guest mole ratios using a modified *dissolution* method,¹⁹ and

they were further characterized using ¹H/¹⁹F/¹³C solids/solution NMR spectroscopy, FT-IR spectroscopy, differential scanning calorimetry (DSC), and PXRD.

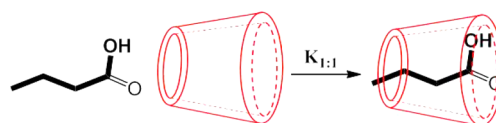
2. EXPERIMENTAL SECTION

2.1. Materials. β-CD hydrate (~10% w/w) and PFBA (98%) were purchased from Sigma-Aldrich Canada Ltd. (Oakville, ON) and were used as received without any further purification. The water content of the materials was determined from thermogravimetric analysis when preparing the sample mixtures.

2.2. Preparation of the Solid β-CD/PFBA ICs. The solid complexes of β-CD/PFC were prepared at the 1:1 and 2:1 host/guest mole ratios using a modified *dissolution* method adapted from a previous report,¹⁹ as depicted in Scheme 1. The solid complexes were ground into fine powders, and upon evaporation of the solvent, the products were analyzed.

2.3. Solution NMR Spectroscopy. ¹H solution NMR experiments were carried out on a three-channel Bruker Avance

Scheme 1. Association of β-CD and PFBA in a 1:1 Host–Guest Stoichiometry Yields a β-CD/PFBA Inclusion Complex



(5 mm DRX probe) spectrometer operating at 500.13 MHz, while the ^{19}F solution NMR spectra were acquired at 282.4 MHz using a 300 MHz Bruker Avance 2 spectrometer outfitted with a 2-channel (H/FX) 5 mm BBO probe. All NMR spectra of samples in solution were prepared in D_2O at host–guest mole ratios of 1:1 and 2:1 at 295 K, in which the chemical shifts (δ) of ^1H and ^{19}F were measured with respect to tetramethylsilane (TMS; ^1H 0.0 ppm) and trifluoroborane (BF_3 ; ^{19}F ~ -131 ppm) as internal standards, respectively. Typical acquisition parameters were as follows: a spectral window of 6250 Hz and a $\pi/2$ pulse width of 8.5 μs for the ^1H spectra; a file size of 64 k data points, a spectral window of 56 818 Hz, and a 10.3 μs ($\pi/2$) pulse width for the ^{19}F spectra. One hundred transients were acquired in all cases, with an acquisition time of 1.15 s, with a file size of 32 k data points and a 1 s relaxation delay.

2.4. Solid-State NMR Spectroscopy. All solids NMR spectra were obtained using a Varian INOVA spectrometer operating in triple-channel HFC mode using a 2.5 mm T3 HFX probe operating at 125.55 MHz for ^{13}C , 499.99 MHz for ^1H , and 469.89 for ^{19}F . Solid-state ^{13}C CP/MAS spectra were referenced externally to adamantane (δ 38.5 ppm) as a secondary standard with respect to TMS. ^{19}F NMR spectra were referenced with respect to hexafluorobenzene (δ , -164.9 ppm) as a secondary standard with respect to CFCl_3 (0 ppm). All samples were spun at the magic angle with a spinning rate of 20 kHz (or as stated) using 2.5 mm zirconium oxide rotors equipped with Vespel (low fluorine background) turbine caps, inserts, and end-caps. All NMR spectra were obtained using a 100 kHz spectral window in transients of 8 k points, which were zero-filled to 64 k, unless stated otherwise. The curve and width parameters for the adiabatic $^1\text{H} \rightarrow ^{13}\text{C}$ CP experiments were set at 50 and 10 000 Hz, respectively, while those for $^{19}\text{F} \rightarrow ^{13}\text{C}$ CP were set at 50 and 50 000 Hz, respectively. Optimal Hartmann–Hahn matching conditions were achieved at a 1 ms contact time and spin locking powers of 68 kHz and 59.5 kHz for the ^{19}F and ^{13}C channels, respectively. ^{13}C spectra of all solid samples were acquired using a two-pulse phase modulation (TPPM) decoupling mode,²⁵ using a pulse phase of 13.5° and decoupling frequencies of 125 and 100 kHz in the ^1H and ^{19}F decoupled channels, respectively, as determined by 360° pulse width measurement in each channel.

2.5. Differential Scanning Calorimetry. DSC experiments were acquired using a TA Q20 thermal analyzer over a temperature range of 30–380 $^\circ\text{C}$. The scan rate was set at 10 $^\circ\text{C}/\text{min}$, and dry nitrogen gas was used to regulate the sample temperature and sample compartment purging. Solid samples were analyzed in hermetically sealed aluminum pans in which the sample masses ranged from 3.50 to 3.80 mg.

2.6. Powder X-ray Diffraction. PXRD spectra were collected using a PANalytical Empyrean powder X-ray diffractometer using monochromatic $\text{Cu K}\alpha_1$ radiation. The applied voltage and current were set to 45 kV and 40 mA, respectively. The samples were mounted in a vertical configuration as evaporated hexane films and PXRD patterns were measured in the continuous mode over a 2θ angle range of $5\text{--}20^\circ$ with a scan rate of 0.5 degree/min.

3. RESULTS AND DISCUSSION

3.1. DSC. DSC and thermogravimetric analysis are complementary techniques that have been used to characterize thermal properties of polymeric²⁶ and other host–guest

systems.^{27,28} Changes in the enthalpy of dehydration of the host due to displacement of cavity water have been used to indicate formation of host–guest complexes.²⁹ The DSC thermograms of the native β -CD hydrate, the 1:1, and 2:1 β -CD/PFBA ICs are depicted in Figure 1. The corresponding

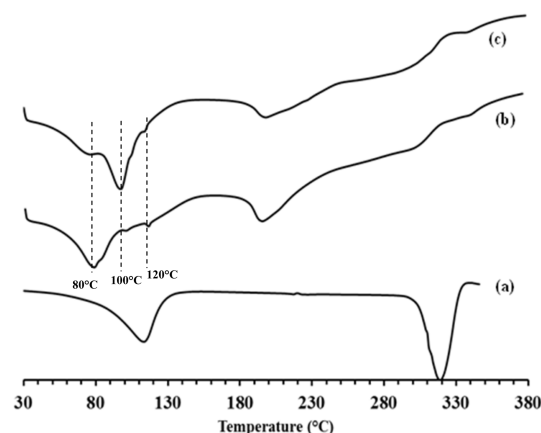


Figure 1. DSC thermograms of (a) β -CD and the (b) 1:1 and (c) 2:1 β -CD/PFBA complexes.

Table 2. DSC Data for β -CD and the 1:1 and 2:1 β -CD/PFBA Inclusion Complexes. Main Dehydration Transitions are Indicated by Asterisks

	dehydration ($^\circ\text{C}$)		vaporization ($^\circ\text{C}$)	decomposition ($^\circ\text{C}$)
β -CD	—	—	113	319
1:1 IC	$\sim 80^*, 90$	~ 102	117	310
2:1 IC	~ 80	$\sim 100^*$	114	310

transition temperatures are listed in Table 2. Generally, the DSC spectra show three major endothermic transitions which are related to dehydration, vaporization, and decomposition processes. The peaks at ~ 115 and 320 $^\circ\text{C}$ (cf. Figure 1a) are related to dehydration and decomposition transitions of the pure host, respectively. The guest molecule in the bound state vaporizes and decomposes at ~ 200 and 310 $^\circ\text{C}$, respectively (Figure 1b,c). The dehydration transitions for the complexes display three endothermic contributions at ~ 80 , 100 , and 120 $^\circ\text{C}$ (cf. Figure 1b,c and Table 2) and exhibit variable hydration levels and nature of the stoichiometry (i.e., 1:1 and 2:1) for the host–guest complexes. It should be noted here that PFBA was reported to form mainly 1:1 host–guest complexes with β -CD in aqueous solution because of *size-fit* complementarity of the host and the guest.³⁰ However, host–guest complexes with other host/guest ratios (e.g., 2:1 and 1:2) may arise in the solid phase.^{31,32} β -CD/PFBA complexes with variable stoichiometric ratios (e.g., 2:1 and 1:2) may result from different binding configurations, e.g., a 2:1 association where the guest is strongly bound by one CD and weakly bound to a second CD macrocycle.

According to Figure 1, the variable enthalpies of dehydration evidenced by the desorption temperatures correlate with different hydration states that exist because of the different guest binding configurations. For example, the displacement of the main dehydration process to lower temperature (80 $^\circ\text{C}$) for the 1:1 complex relative to the 2:1 complex (~ 100 $^\circ\text{C}$) may be

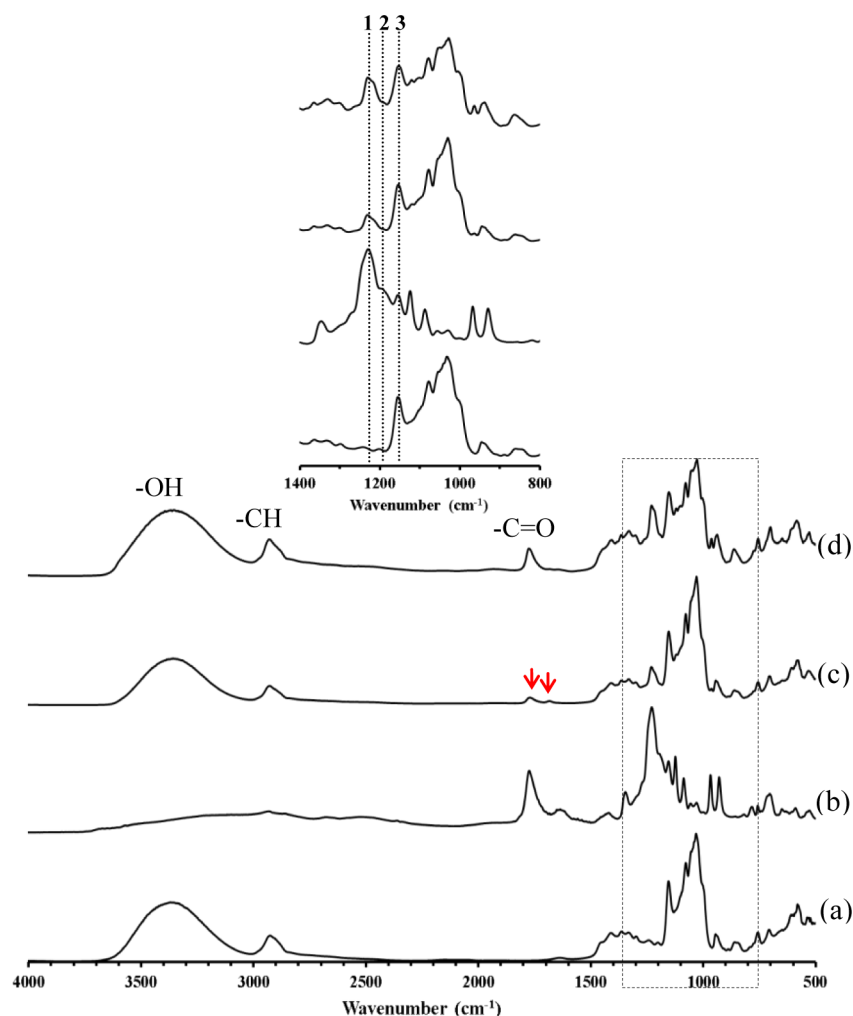


Figure 2. FT-IR for (a) native β -CD, (b) PFBA, and the (c) 1:1 and (d) 2:1 β -CD/PFBA inclusion complexes. Inset: expanded region from 1400 cm^{-1} to 800 cm^{-1} .

associated with a reduced contribution of cavity-bound water because of its removal upon guest binding. The host cavity for the 1:1 complex is fully occupied by the guest molecule. Moreover, the deconvolution of the broad DSC peak for the 1:1 complex at $\sim 80^\circ\text{C}$ displays a shoulder at higher temperature ($\sim 90^\circ\text{C}$), and this may suggest an additional guest microenvironment in this complex. In contrast, the 2:1 host–guest association reveals a greater level of H-bound water because of the greater mole fraction of the host. Hence, the dehydration process shifts to higher temperature (100°C). A minor enthalpic contribution at a temperature corresponding to the main dehydration process for the 1:1 complex ($\sim 80^\circ\text{C}$) is displayed for the 2:1 complex, suggesting minor contributions of the 1:1 guest configuration for this complex. When compared to the vaporization temperature of pure PFBA (bp 120°C , cf. Table 1), the vaporization temperature of the guest in the bound state is increased (195 – 198°C), providing thermodynamic evidence of the formation of stable inclusion compounds. The minor transitions at 120°C for the complexes may be related to the melting of small amounts of noninclusion bound, unbound (free) PFBA guest, or hydrate water.

3.2. FT-IR Spectroscopy. FT-IR spectroscopy has been widely used to study the structure of CD-based ICs in which the guest molecule bears a carbonyl group because the CO-stretching band is sensitive to changes in guest conformation as

well as possible H-bonding with the CD.^{33,34} The FT-IR spectra of the host, guest, and the 1:1 and 2:1 β -CD/PFBA ICs are shown in Figure 2. The relative intensities of the --OH ($\sim 3400\text{ cm}^{-1}$), --CH ($\sim 2900\text{ cm}^{-1}$) and --C=O ($\sim 1700\text{ cm}^{-1}$) vibrational bands for the 1:1 (weaker) and 2:1 (stronger) inclusion complexes (Figure 2c,d) correlate with the relative mole ratios of the host/guest relative to the unbound species. The unbound PFBA is characterized by a broad, low intensity --OH band ~ 3600 – 2500 cm^{-1} that is typical of fatty acids.³⁵ The attenuation of the carbonyl band in the 1:1 and 2:1 complexes is related to H-bond formation and supports the formation of β -CD/PFBA inclusion complexes. The visibly attenuated carbonyl band in the 1:1 complex (Figure 2c) indicates formation of multiple H-bonds,³⁶ as this band displays two distinct contributions. The IR results further support that the guest exists in the 1:1 complex in two distinct microenvironments, in agreement with the DSC results in Figure 1.

The FT-IR spectral region from ~ 1400 – 800 cm^{-1} is of interest in terms of the conformational preference of the guest molecule. This expanded FT-IR region is shown as an inset in Figure 2. Bands 1 ($\sim 1230\text{ cm}^{-1}$), 2 (1200 – 1210 cm^{-1}), and 3 (1150 cm^{-1}) in the expanded region of Figure 2 were reported previously^{17,37} and assigned to the CF_2 asymmetric stretching mode, CC bending and CCC stretching modes, and CF_2 symmetric stretching modes, respectively. Note that the

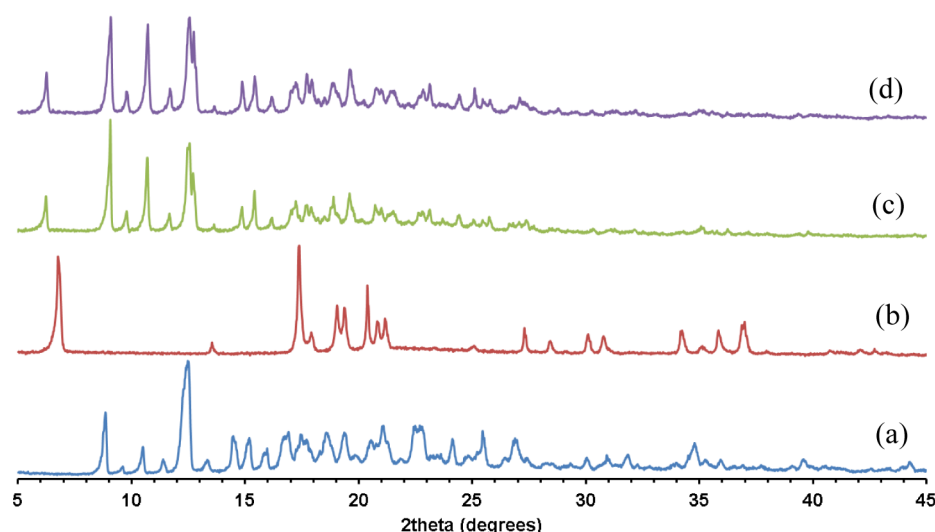


Figure 3. PXRD patterns for (a) native β -CD, (b) SPFB, and the (c) 1:1 and (d) 2:1 β CD/PFBA inclusion complexes.

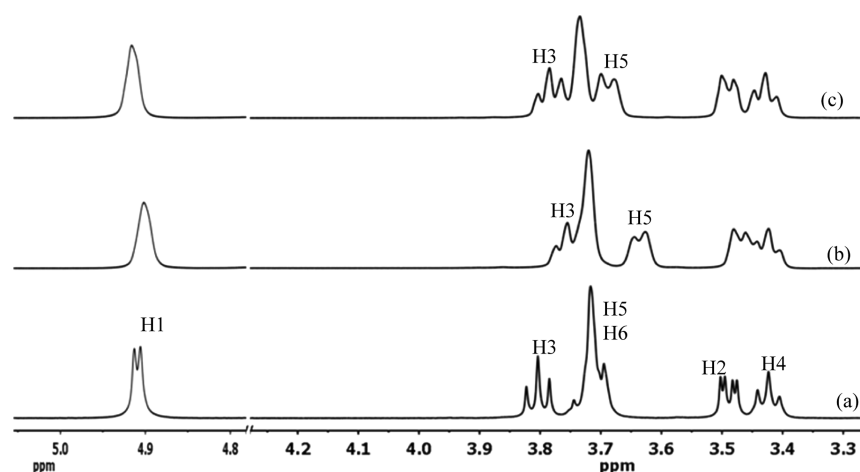


Figure 4. ^1H solution NMR spectra of (a) β -CD and the (b) 1:1 and (c) 2:1 β -CD/PFBA inclusion compounds in D_2O at 295 K.

wavenumber position of band 2 is not straightforward to assign as this band may be partly overlapped with band 1. However, such band position is assigned to be within $1200\text{--}1210\text{ cm}^{-1}$ range. Changes in the relative intensities of these bands, particularly band 2, were related to the *trans* and *gauche* conformations of the PFC chain. As described previously, perfluorocarbon chains ≤ 8 carbons (e.g., PFBA) generally adopt a fully zigzag (*trans*) conformation in the solid phase,³⁸ whereas composite zigzag or helical conformations were reported for C8–C12 chains.³⁹ Ellis et al.⁵ reported an NMR simulation of coupling constants in which the PFBA chain in solution does not adopt a fully *trans* conformation. However, such conformation is the generally accepted form of C4 perfluorocarbons in the solid phase.⁴⁰

Bands 1–3 in Figure 2 were observed for gaseous $n\text{-C}_4\text{F}_{10}$ where band 2 ($1200\text{--}1210\text{ cm}^{-1}$) was attributed to the *trans*-conformer.⁴⁰ A decrease in intensity of this band was previously attributed to a *trans*-to-*gauche* conformational change of the perfluorocarbon chain. Recall that PFBA adopts a full *trans* conformation in its unbound form in the solid state. However, a variable conformation may result if the environment of the guest is varied.

Erkoc and Erkoc³ reported that the conformation of PFOS changed from helical to near-linear (zigzag) when H was

replaced with F because of changes in the dipole moment of the various molecular fragments. Similarly, the conformation of PFOA changed from a helical to zigzag when packed into a periodic lattice.³⁹ We believe that the significant decrease in the intensity of band 2 for the β -CD/PFBA complexes is related to the *trans*-to-*gauche* conformational change of the perfluorocarbon chain. The guest molecule in the 1:1 and 2:1 complexes is expected to adopt variable conformation with variations in the CF_2 symmetric stretching modes (band 1) and CC bending/CCC stretching modes (band 2), according to the FT-IR results.

3.3. PXRD. The PXRD patterns for the host and the 1:1 and 2:1 host–guest complexes prepared by the modified *dissolution* method are shown in Figure 3. The PXRD of sodium perfluorobutyrate (SPFB) is shown for comparison because it is the salt form of the conjugate base of PFBA. The hydrate form of the host (β -CD) exhibits intense diffraction lines at lower 2θ values ($\sim 9^\circ$, 12°) and minor signatures at higher 2θ that are characteristic of a “cage-type”⁴¹ crystalline structure. SPFB exhibits intense diffraction lines $\sim 7^\circ$ and $\sim 17\text{--}22^\circ$ with minor reflections at higher 2θ values. The diffraction patterns of the 1:1 and 2:1 complexes (Figure 3c,d) consist of 2θ values $\sim 6^\circ$ and $9\text{--}13^\circ$, where the higher 2θ region is comprised of minor reflections that are characteristic of cage-type structures.

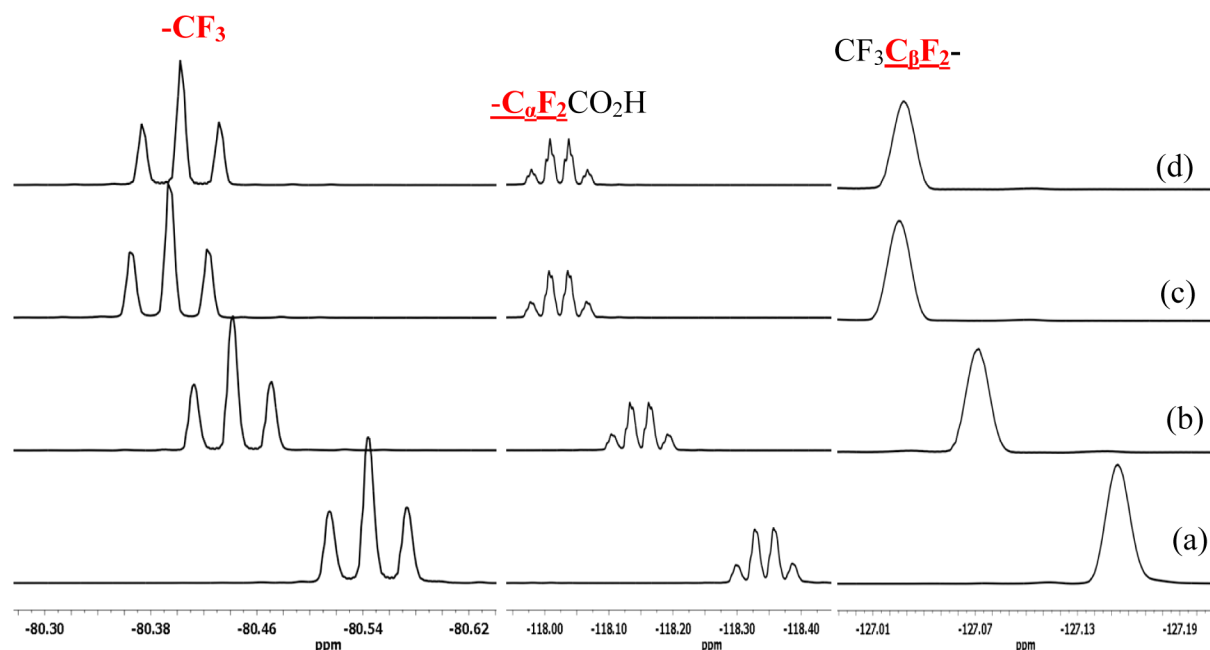
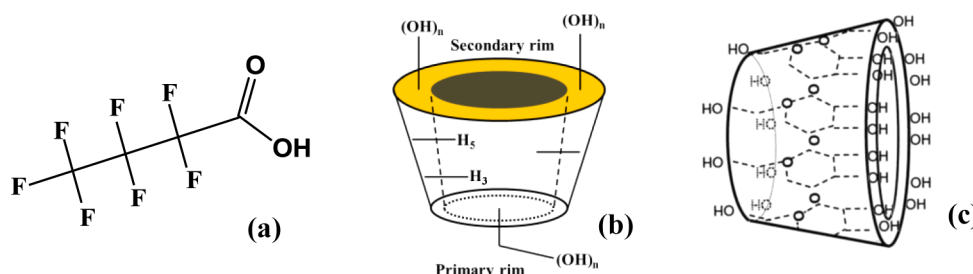


Figure 5. ^{19}F solution NMR spectra of (a) PFBA and the (b) 1:2, (c) 1:1, and (d) 2:1 β -CD/PFBA inclusion compounds in D_2O at 295 K.

Scheme 2. Molecular Structure of (a) PFBA and (b,c) β -CD^a



^aThe structure of β -CD is shown as a truncated toroid in which the primary and secondary hydroxyls and glycosidic oxygen bridges are shown. The intracavity protons (H_3/H_5) are shown in panel b.

We conclude that β -CD forms cage-type structures with PFBA, similar to its structure in the native unbound form. The relative shift and intensity of 2θ reflection at $\sim 6^\circ$ in the 1:1 and 2:1 complexes with respect to pure SPFB (at 7°) reveal the variable conformations and configurations of the guest in these complexes.

3.4. ^1H and ^{19}F Solution NMR Spectroscopy. ^1H and ^{19}F solution NMR spectroscopy were used to characterize the inclusion compounds of β -CD and PFBA through complexation induced shifts (CIS), as shown in Figures 4 and 5, respectively. In Figure 4, the ^1H solution NMR spectra for β -CD (a) and the 1:1 (b) and 2:1 (c) β -CD/PFBA inclusion compounds are shown. The ^1H solution NMR spectra were assigned according to literature reports.⁴² The intracavity protons (i.e., H_3 and H_5 , cf. Scheme 2b) are the most affected nuclei, providing evidence for the formation of inclusion compounds between β -CD and PFBA. The H_3 and H_5 CIS values are greater in the 1:1 complex, and this is related to the greater steric effect on the intracavity nuclei upon complexation. It should be noted here that the complexation-induced shift is a weighted average due to the bound and unbound species.⁴³ The observed chemical shift changes for the extracavity ^1H nuclei (i.e., H_1 , H_2 , H_4) in the 1:1 and 2:1 complexes may be associated with the extracavity environment

of the PFBA guest in these complexes or possibly the complexation-induced conformational change of the host. The extracavity environment (e.g., H_1) experiences variable steric effects from the guest in the 1:1 complex (shielding) versus the 2:1 complex (deshielding). The shielding and deshielding effects of the 1:1 and 2:1 complexes may be related to the variable conformations of the guest as described in the FT-IR results. The increase in line broadening upon complexation can be readily ascribed to the increase in correlation times expected upon complexation, which decreases T_2 , leading to a wider natural line width. The greater line width further supports the formation of the complexes.

We believe that the guest molecule preferentially adopts the *gauche* conformation in the 1:1 complex in solution phase, whereas a fully *trans* conformation is favored in the 2:1 complexes. A *gauche* conformation is anticipated to impart a greater steric strain (shielding) on the host compared to a fully *trans* conformation, in agreement with the ^1H solution NMR results.

Figure 5 shows the expanded ^{19}F solution NMR spectra of PFBA (a) and the β -CD/PFBA inclusion compounds prepared at the 1:1 (b) and 2:1 (c) mole ratios. Similar results for the 1:2 host–guest preparation were included for comparison. The assignment of the ^{19}F solution NMR agrees well with previous

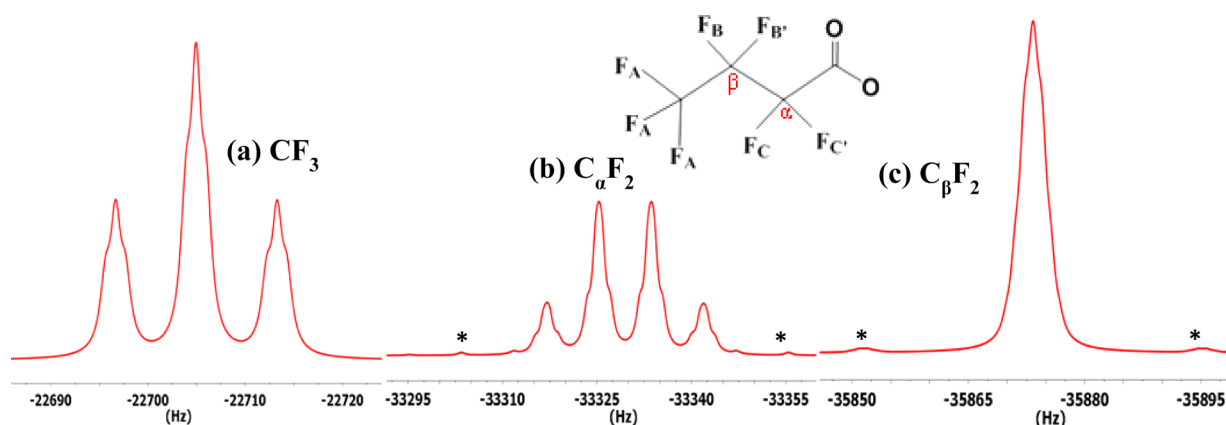


Figure 6. ^{19}F simulated spectrum of PFBA (Hz) in D_2O at ambient temperature showing the splitting of the (a) $-\text{CF}_3$, (b) $\alpha\text{-CF}_2$, and (c) $\beta\text{-CF}_2$ signals. The satellite lines are indicated by asterisks.

literature reports.⁵ The formation of host–guest ICs results in an overall downfield shift of the ^{19}F resonances due to the reduced polarizability of the host interior relative to the environment of bulk aqueous solution.⁴⁴ This provides evidence for the formation of $\beta\text{-CD/PFBA}$ inclusion compounds in solution. Note that the CIS values did not increase further beyond the 1:1 mole ratio, supporting the fact that PFBA forms mainly 1:1 complexes with $\beta\text{-CD}$ in solution phase. The CIS values for the 1:2 host–guest complexes are the least affected relative to unbound PFBA and may be due to the lower mole ratio of the host.

The inherent line widths in the spectra of Figure 5 are about 1 Hz, where slight distortions due to differences in shimming cause slight line shape changes between samples which could easily be confused for subtle changes in the splitting patterns between the complexes and pure PFBA. As one follows the ^{19}F shifts of all the signals, one realizes that the trend is the increase in δ of the ^{19}F resonance lines with the degree of complexation. This can not only be ascribed to the effect of the host entirely, but also is evidence of the guest conformational changes occurring. According to the IR results, the guest molecule adopts the *gauche* conformation in the complexed state. However, because such results clearly suggest that the *trans* contribution in the complexed form increases with the degree of complexation (i.e., 2:1 > 1:1), we should expect to see a reduction in the *gamma-gauche* shielding effect. As a result the chemical shift should increase from the 1:2 through the 1:1 to 2:1 host–guest complexes (i.e., Figure 5b–d).

^{19}F NMR in solution can be a very important tool in understanding the structure of perfluorocarbon materials. For example, the ability to discern the coupling constants of all the ^{19}F nuclei in highly fluorinated materials in liquid form is an important technique in determining and understanding molecular dynamics and conformation of such materials. Coupling constants in perfluorinated carboxylic acids have largely been indiscernible because of long-range coupling (over 4 bonds) and coincidental spectral overlap.^{45,46} The ^{19}F solution spectrum of PFBA in D_2O was simulated using MestreNova to determine the individual coupling constants. The simulated spectrum of pure PFBA in D_2O along with its labeled structure are shown in Figure 6.

The spectrum of PFBA can be determined by seven coupling constants: $^4J_{\text{AC}} = ^4J_{\text{AC}'} = 8.3$ Hz, $^3J_{\text{AB}} = 1.4$ Hz, $^3J_{\text{AB}'} = 0.7$ Hz, $^3J_{\text{BC}} = ^3J_{\text{B'C}'} = 6.9$ Hz, $^3J_{\text{B'C}} = ^3J_{\text{BC}'} = -5.8$ Hz, $^2J_{\text{BB}'} = -263.1$ Hz, and $^2J_{\text{CC}'} = -283.1$ Hz. The values of coupling constants

reported herein agree well with reported values in the literature;⁴⁷ however, at this resolution they cannot represent a unique solution. According to the splitting pattern, the ^{19}F spectra of pure PFBA and the complexes in D_2O are $\text{A}_3\text{BB}'\text{CC}'$ spin systems in which the CF_2 groups are magnetically inequivalent. Figure 7 represents the three possible rotamers

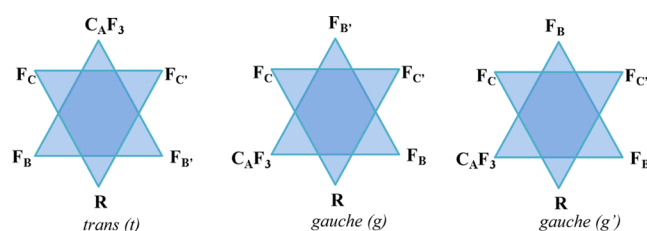


Figure 7. Three possible rotamers of perfluorobutyric acid (PFBA).

of PFBA; one *trans* (*t*) and two equivalent *gauche* (*g*, *g'*) conformers. Note that fast rotational averaging on the NMR time scale in solution at ambient temperature is such that the spectrum of PFBA is represented by spectral parameters which are averages of the chemical shifts and coupling constants in the three rotational isomers, weighted according to their populations. Therefore, the couplings do not reflect a single configuration, but an average over all three rotamers,⁴⁸ which in this case constitute one: *trans* and two symmetrically equivalent *gauche* configurations.

The $\text{F}_\text{B}/\text{F}_{\text{B}'}$ and $\text{F}_\text{C}/\text{F}_{\text{C}'}$ spins are strongly coupled by two geminal couplings whose difference ($^2J_{\text{BB}'} - ^2J_{\text{CC}'}$) is 20 Hz. This resonance spacing (i.e., ~ 20 Hz) can be seen occurring between the satellite lines and the main signals in both subspectra (cf. Figure 6b,c). These are second-order satellites, which can result only from very strong coupling. A second set of such satellites (at very low intensity) should appear in the spectrum of Figure 6b (not shown in the scale) for the $\text{C}_\alpha\text{F}_2$ group at ~ 546.2 Hz. Hence, the 2J couplings are -283.1 and -263.1 Hz. Reported geminal couplings in acyclic $-\text{CF}_2-$ groups range between 260 and 290 Hz.⁴⁹

The coupling constants cannot be determined from the splitting observed in the BB' and CC' as the individual spectral lines are not resolved; however, some splittings observed can be attributed to the sum of the various geminal and vicinal coupling constants. Hence, the inability to obtain a unique solution for the spectral parameters (spectral resolution of less than 0.3 Hz would be required in this case). For example, the

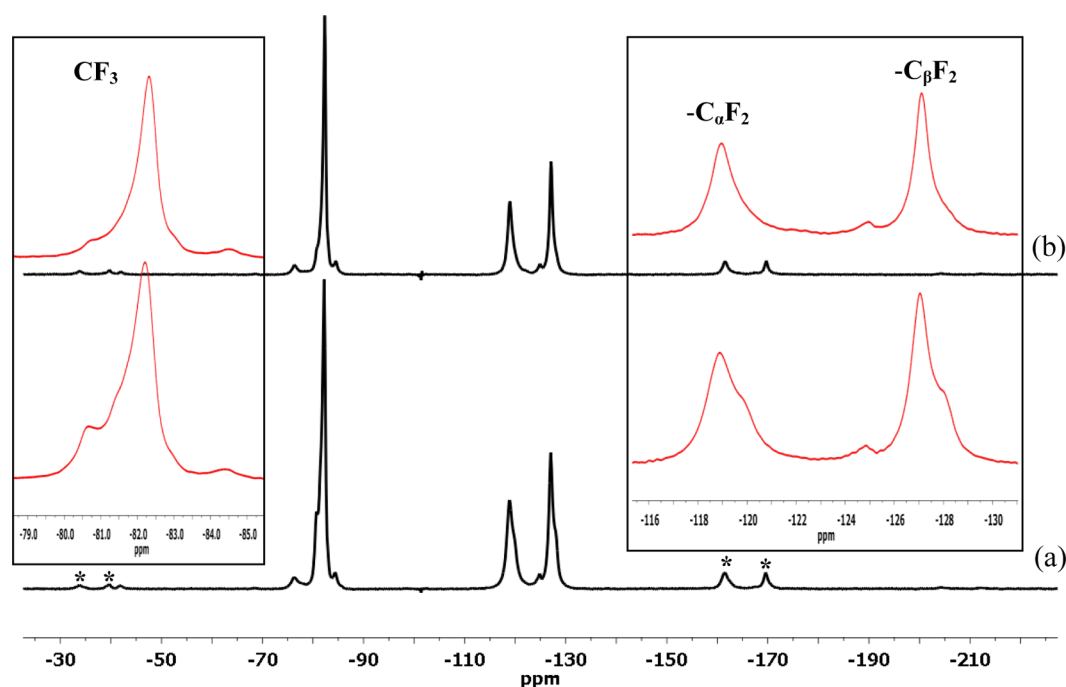


Figure 8. ^{19}F DP NMR spectra of the (a) 1:1 and (b) 2:1 β -CD/PFBA complexes acquired at 20 kHz MAS and 295 K.

$^3J_{\text{AB}}$ and $^3J_{\text{AB'}}$ couplings add up to 2.1 Hz. The two couplings do not have to be equal, so any combination that adds up to 2.1 Hz is valid up to a limit determined by the two germinal couplings. Similarly, the sum of the two vicinal couplings $^3J_{\text{BC}}/^3J_{\text{B'C'}}$ and $^3J_{\text{B'C'}}/^3J_{\text{BC}}$ is 1.1 Hz. Again, these couplings cannot be determined separately at this resolution. Resolution enhancement allowing the identification of some characteristic spacings in the $\text{F}_{\text{CC'}}$ regions places $^3J_{\text{BC}}$ and $^3J_{\text{B'C'}}$ at 6.9 and -5.8 Hz. The $^4J_{\text{AC}}$ and $^4J_{\text{AC'}}$ couplings add up to 16.6 Hz. Again, these couplings cannot be determined separately at this resolution. They do not have to be equal; however, in the simulation they were assumed to be equal at 8.3 Hz. Changing the magnitudes of 4J couplings but preserving their sum does not change the appearance of the A3 and CC' regions in the spectrum up to a limit determined by the two germinal couplings.

The nearly constant splitting patterns between all the ^{19}F spectra of neat PFBA and its complexes cannot be used as evidence for the lack of conformational changes occurring upon complex formation, as any change that preserves the sums of the 3J couplings will have the same pattern. As the 3J couplings are an average of their counterparts in the individual rotamers (i.e., t , g , and g' , cf. Figure 7), they will change only subtly upon stabilization of the *trans* conformation. Thus, the sum of these couplings cannot be expected to increase significantly. The interpretation of the splitting pattern of PFBA reveals that the F atoms on the CF_2 groups are nonequivalent, as indicated in a previous report.⁵ Thus, the results suggest that there must be fast rotation about the CF_2 – CF_2 bonds of PFBA chain in aqueous solution, but each configuration (i.e., t , g , and g') does not contribute equally. Therefore, the main chain cannot be rigid, because if it were, one would expect to observe the subspectra corresponding to all three rotamers. Note also that the *trans* configuration is likely to be the least stable, compared to the two *cis* (*gauche*) configurations, which have equal populations as they have the same energy. Thus, as the *trans* configuration is stabilized, the average 3J and 4J reflect this by

an increased contribution from the coupling constants in the *trans* rotamer to the average. This leads to the conclusion that the PFBA chain undergoes free rotation of the $-\text{CF}_3$ group about the 3-fold axis and appreciable rotation about the CF_2 – CF_2 bonds of the main chain. The structure of PFBA in the complexed form in the solid state is expected to vary, especially with respect to its bond rotation dynamics, which may be influenced by steric interactions with the host. ^{19}F DP/MAS NMR and dynamic relaxation results are presented to further understand the structure and dynamic properties of PFBA and its complexes with β -CD, respectively.

3.5. ^{19}F DP/MAS NMR Spectroscopy. NMR methods in which the nucleus of interest is observed provide an opportunity to study the structure of host–guest systems. Figure 8 shows assigned ^{19}F DP/MAS solid NMR spectra of the 1:1 and 2:1 solid complexes prepared by the modified dissolution method. The ^{19}F DP/MAS spectrum of the guest was not acquired because PFBA is a liquid at room temperature. Minor changes in the CIS values for the methyl (CF_3) and methylene (CF_2) groups in the 1:1 and 2:1 β -CD/PFBA complexes reveal variable environments and dynamics of the guest as previously described.

The ^{19}F resonance lines of the 1:1 and 2:1 complexes are characterized by various contributions which may be due to the presence of various microenvironments of the guest and/or the presence of unbound guest. Note that the fast rotation of the short chain PFBA guest, particularly the CF_3 group as described in the simulation studies, affects the line width and shape of the adjacent ^{19}F lines. The motional dynamics of the PFBA chain are generally expected to be much faster compared to that of C8 (e.g., PFOA and SPFO) perfluorocarbon chains. In Figure 8, the CF_3 group displays the sharpest resonance line followed by the methylene group connected directly next to it (C_βF_2) and then the CF_2 group connected next to the carbonyl group ($\text{C}_\alpha\text{F}_2$). The ^{19}F resonance lines of the 1:1 complex reveal prominent line shape features compared to the 2:1 complex and may suggest variable guest binding configurations

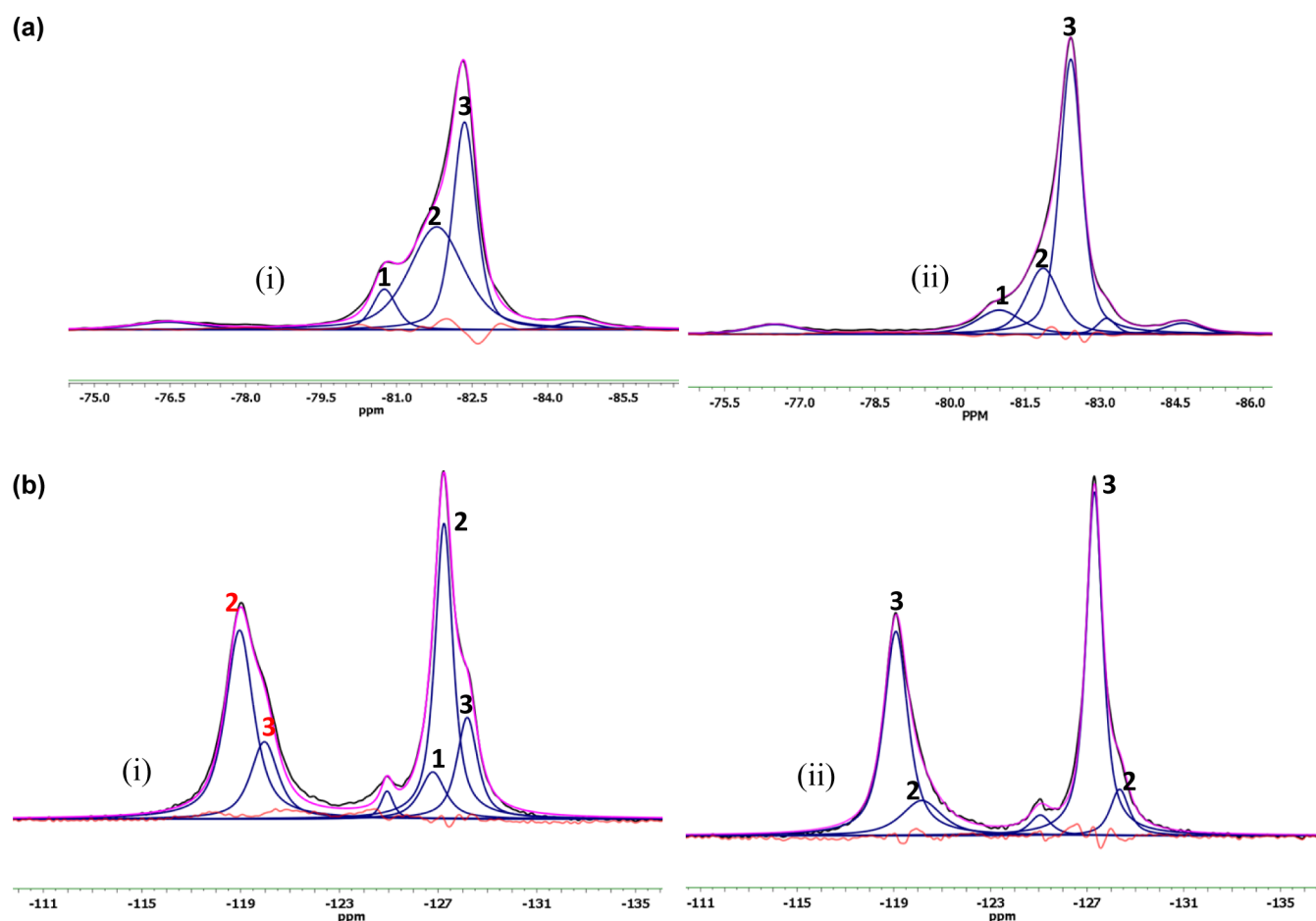


Figure 9. (a) Deconvolution analyses of the CF_3 line shapes for the ^{19}F DP/MAS 20 kHz spectra of the (i) 1:1 and (ii) 2:1 β -CD/PFBA solid complexes at 295 K. (b) Deconvolution analyses of the CF_2 line shapes for the ^{19}F DP/MAS 20 kHz spectra of the (i) 1:1 and (ii) 2:1 β -CD/PFBA solid complexes at 295 K.

consistent with the results from DSC and FT-IR spectroscopy. Deconvolution analyses of the ^{19}F resonance lines were carried out to further understand the structure of the complexes and the dynamics of the guest.

3.6. Deconvolution Analyses of ^{19}F NMR Line Shapes.

Deconvolution analyses of NMR line shapes were previously used to assign the various phases (e.g., crystalline and amorphous) of a compound.⁵⁰ The deconvolution results for the CF_3 and CF_2 lines at 295 K appear in panels a and b of Figure 9 for the 1:1 and 2:1 complexes, respectively. The CF_3 and CF_2 resonances of the 1:1 and 2:1 complexes are generally characterized by two or three components (1–3, cf. Figure 9a,b). In a previous report,¹⁹ three topologies of β -CD/PFOA complexes were concluded from the deconvolution analyses of the CF_3 lineshapes. These topologies corresponded to a 1:1 β -CD/PFOA complex in which two configurations (CF_3 -out of and CF_3 -in cavity) were possible and a 2:1 complex with a CF_3 -in cavity configuration (cf. Scheme 2, ref 19). The three topologies (two for the 1:1 complex and one for the 2:1 complex) reported for β -CD/PFOA complexes were determined by the length of the perfluorocarbon chain (~ 15 Å) with respect to that of the CD cavity (~ 7.9 Å). In the case of β -CD/PFBA complexes, higher-order stoichiometries (e.g., 2:1 and 1:2) may arise in the solid phase, in addition to the 1:1 stoichiometry, indicating that a number of binding configurations are possible, as suggested by DSC, FT-IR, and ^{19}F DP/MAS NMR results. As was the case with the β -CD/PFOA

complexes, the different binding configurations formed by PFBA with β -CD are determined by the *size-fit* complementarity (length of PFBA is about half that of PFOA) and interactions between the different components of the host and guest. For example, the edges of β -CD are lined with hydroxyl groups, whereas the internal cavity is lined with H atoms and glycosidic O bridges (cf. Scheme 2c). Therefore, the internal cavity is hydrophobic, whereas the annular hydroxyl groups are hydrophilic in nature. Several binding interactions are therefore possible between the perfluorinated carboxylate anion and the various segments of the macrocycle.

The relative distribution of components 1–3 for the CF_3 and CF_2 groups in the 1:1 and 2:1 complexes were estimated from the deconvolution parameters, and reveal variable binding geometries and stoichiometries in these complexes. Deconvolution parameters showing chemical shifts, areas under curves, and relative Lorentzian/Gaussian ratios are presented as Supporting Information. Whereas component 2 is more prominent in the 1:1 complex, the 2:1 complex is mainly defined by component 3. On the other hand, component 1 is the least prominent in both the 1:1 and 2:1 complexes and may be missing entirely in the latter. Thus, we conclude that components 1–3 may correspond to guest binding configurations that resemble 1:2 (1), 1:1 (2), and 2:1 (3) host/guest stoichiometries, respectively. Scheme 3 represents the various possible binding configurations of PFBA within the CD cavity. Note that guest penetration through the narrow rim is possible.

Scheme 3. Schematic Representation of the Binding Interaction Postulated for PFBA Guest and β -CD; (1) Partial Guest Inclusion in a 1:2 Host/Guest Ratio; (2) Complete Guest Inclusion in a 1:1 Host/Guest Ratio; and (3) Complete Inclusion with Guest Protruding to Result in 2:1 Host/Guest Ratio; Note Inclusion through the Narrow Rim of CD is Possible



As well, formation of channel or cage structures, as described in the PXRD results, are known to occur in CD complexes but are omitted for clarity.

Configuration 1 in Scheme 3 is the least stable from a thermodynamic point of view and may represent a 1:2, or more accurately a 0.5:1 host/guest stoichiometry, but may also represent a free guest. According to the deconvolution analyses (cf. panels a-i and b-i of Figure 9), the 1:1 preparation gives rise to approximately equimolar amounts (refer to Table SI-1 of Supporting Information) of 1:1 (configuration 2) and 2:1 (configuration 3) host/guest stoichiometries and small amounts of the 1:2 stoichiometry (configuration 1). The presence of the 1:1 and 2:1 complexes in the 1:1 preparation may coincide with the two DSC dehydration transitions at ~ 80 and 90 $^{\circ}\text{C}$, respectively. In contrast, the 2:1 preparation is composed primarily of the 2:1 complex, with a small contribution of the 1:1 host/guest complex (cf. panels a-ii and b-ii of Figure 9), consistent with the minor DSC dehydration transition at ~ 80 $^{\circ}\text{C}$. The 1:2 host/guest contributions are either attenuated or are missing entirely in the 2:1 preparation because of the greater mole fraction of the host. The presence of appreciable amounts of the 1:2 contributions in the 1:1 preparation is consistent with the greater mole ratio of the guest and may suggest the presence of a free guest in this preparation. The hydration and H-bonding

behavior described in the DSC and FT-IR results, respectively, agree well with the findings of the deconvolution analyses. Preparations with variable host/guest configurations in which different stoichiometric distributions (i.e., 2:1, 1:1, and 1:2) may be present are expected to experience different hydration and H-bonding effects.

3.7. $^1\text{H} \rightarrow ^{13}\text{C}$ CP/MAS NMR Spectroscopy. Multinuclear NMR techniques employing polarization transfer have been used to provide unequivocal evidence for the formation inclusion complexes.^{51–53} Additionally, solid-state ^{13}C NMR CIS values and line shape variations can be used to probe conformational effects and molecular dynamics of host–guest systems.⁵⁴ The NMR spectra of the native β -CD and the 1:1 and 2:1 host–guest inclusion compounds obtained using $^1\text{H} \rightarrow ^{13}\text{C}$ CP under conditions of 20 kHz MAS at ambient temperature are depicted in Figure 10. The ^{13}C resonance lines were assigned in agreement with previous reports.^{53,55} The individual ^{13}C nuclei for β -CD hydrate (Figure 10a) are not completely resolved because of the amorphous nature and variable hydration state of the material, in addition to the spectral overlap of certain ^{13}C resonance lines. Note that the $^1\text{H} \rightarrow ^{13}\text{C}$ CP/MAS NMR spectra in Figure 10 show ^{13}C host nuclei and because the guest has no protons, any changes in line shape and width are attributed to hydration properties of the 1:1 and 2:1 complexes. Therefore, the extent and nature of hydration is influenced by the guest binding configuration in these complexes. CIS patterns similar to those observed in solution ^1H NMR are observed in the ^{13}C solid NMR results, further supporting the presence of variable hydration states and guest motional dynamics. The most attenuated CIS values are observed in the spectrum of the 1:1 complex for the intracavity carbon nuclei (i.e., C_3 and C_5). This further supports the inclusion of the guest within the cavity. The deshielding pattern in the 2:1 complex reveals less steric hindrance of the guest for the intracavity nuclei compared to the 1:1 complex (shielding). As well, there are prominent chemical shift changes to lower field in the 2:1 complex for the framework carbon nuclei (C_1 and C_4), whereas the chemical shift (δ) of C_6 is unaffected in

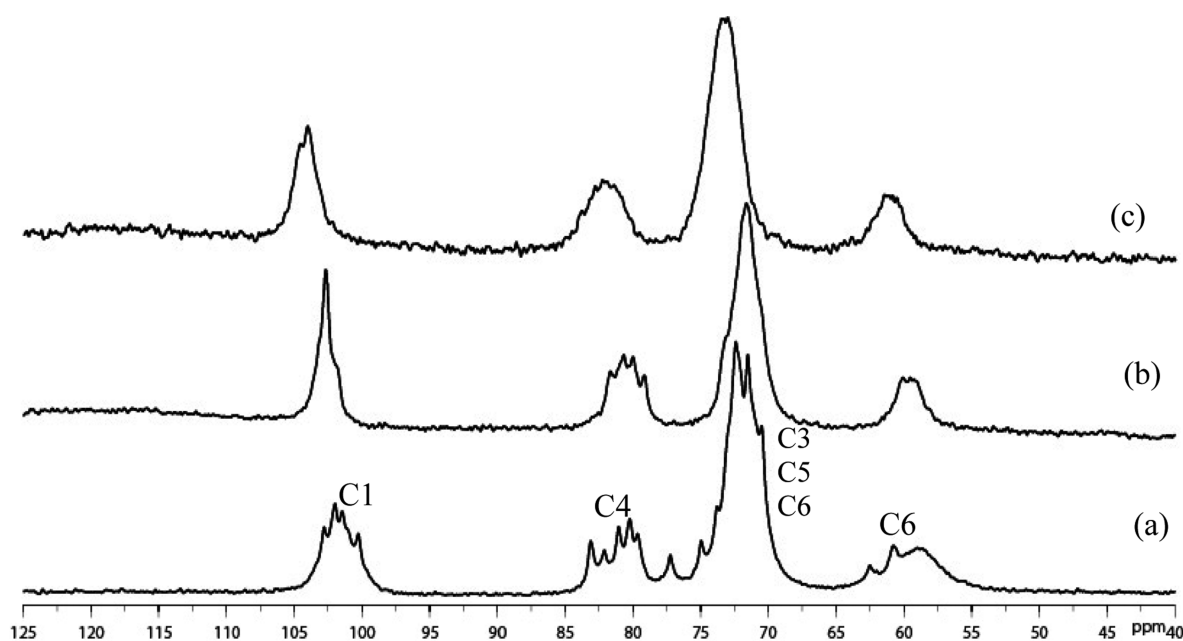


Figure 10. ^{13}C $^1\text{H} \rightarrow ^{13}\text{C}$ CP NMR results for (a) β -CD and the (b) 1:1 and (c) 2:1 β -CD/PFBA complexes at 20 kHz MAS and 295 K.

both complexes. In general, the 1:1 complex experiences reduced δ for almost all of its ^{13}C nuclei. We infer from the ongoing discussion that the host cavity in the 1:1 complex experiences greater steric effects from the included guest compared to the 2:1 complex. We conclude that the guest molecule may adopt a *trans* conformation in the 2:1 complex as compared to a *gauche* conformation in the 1:1 complex, in accordance with the configurations in Scheme 3 and the IR and solution NMR results. Variations in the relative intensities of IR bands 1 (ν_s/CF_2) and 2 (β/CC and ν/CCC) were observed for the 1:1 and 2:1 complexes and may be related to differences in the conformation of the guest in these compounds. A near-linear conformation of the guest in the 2:1 complex is generally expected to cause minimal constraints on the host framework, thereby resulting in a downfield shift for such ^{13}C nuclei.

The spectrum of the 1:1 complex (Figure 10b) is characterized by narrow resonance lines, whereas the resonance lines for the 2:1 complex are relatively broad (Figure 10c). The observed differences in line width may be due to differences in guest dynamics. The guest molecule in the 1:1 complex is expected to be more dynamic than that in the 2:1 complex in which the guest may be completely encapsulated by two host macromolecules. In the case of the 1:1 complex, part of the guest may extend outside of the CD cavity as shown in Scheme 3. The deshielding effect observed for the extra- and intracavity carbon nuclei of the host in the 2:1 complex may be related to a variable guest conformation, as described above, and in agreement with FT-IR and solution and solid NMR results. For PFBA to form a 2:1 host/guest complex with CD, the guest must adopt a near-linear conformation. We conclude that while PFBA guest adopts a *gauche* conformation in the 1:1 (and 1:2) host/guest complexes, the conformation in the 2:1 complex is not *gauche* but a linear one.

3.8. $^{19}\text{F} \rightarrow ^{13}\text{C}$ CP/MAS NMR. $^{19}\text{F} \rightarrow ^{13}\text{C}$ CP/MAS NMR techniques allow for dipolar interactions between the host and guest to be detected. Figure 11 shows the $^{19}\text{F} \rightarrow ^{13}\text{C}$ CP/MAS

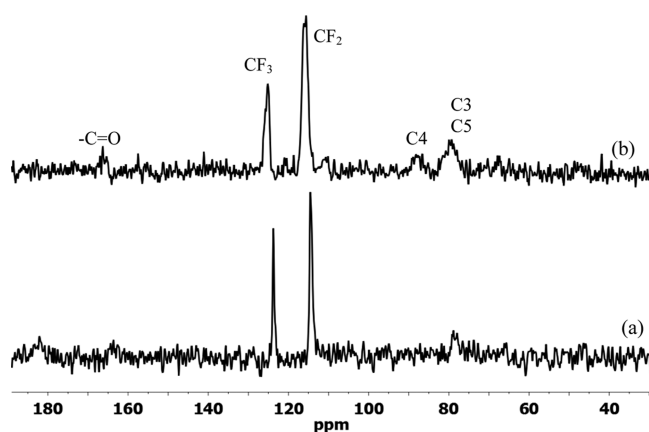


Figure 11. ^{13}C $^{19}\text{F} \rightarrow ^{13}\text{C}$ CP/MAS NMR results for the (a) 1:1 and (b) 2:1 β -CD/PFBA complexes at 20 kHz MAS and 295 K.

NMR spectra of the host/guest complexes prepared at variable mole ratios (i.e., 1:1 and 2:1) assigned according to spectra of Figures 5 and 10. The ^{13}C resonance of the carbonyl group for the β -CD/PFBA inclusion compounds is observed at a much higher field ($\delta \sim 160$ ppm) compared to $\delta \sim 170$ ppm for the carbonyl carbon of the PFOA complexes in a previous study.¹⁹ Carbonyl carbon nuclei in general resonate in the characteristic region between 150–220 ppm, whereas carbonyl groups of

carboxylic acids appear in the range of 160–180 ppm.⁵⁶ The observed δ value for the carbonyl carbon of PFBA reported herein is in good agreement with a reported value in solution by ^{13}C NMR.⁵⁷ The most remarkable observation in the $^{19}\text{F} \rightarrow ^{13}\text{C}$ CP/MAS results is the appearance of a host signal centered at ~ 78 ppm. This signal indicates that ^{19}F polarization from the guest has been transferred to the ^{13}C nuclei of the host cavity (i.e., C_3 and C_5) and provides unequivocal evidence for the inclusion of the PFBA guest within the host cavity. The relative intensities of this signal for the 1:1 (low) and 2:1 (high) complexes reveals a more efficient polarization transfer for the latter, and this is related to the differences in guest conformation and dynamics in the two complexes. The appearance of a similar resonance at ~ 85 ppm (i.e., C_4) for only the 2:1 complex further supports an altered binding configuration and conformation of the guest in this product. Note that C_4 is closer to the center of the CD macrocycle and supports complete encapsulation in the 2:1 complex.

The dynamics and conformation of the guest in the 2:1 complex contribute to more efficient polarization transfer, as evidenced from the greater intensity of the resonance at ~ 78 ppm. The guest molecule in the 2:1 complex is believed to adopt a near-linear conformation, in which the guest is entirely encapsulated within the host cavity space as described above. In the case of the 1:1 complex, the *gauche* conformation coupled with faster dynamics of the guest are expected to reduce efficient dipolar coupling between the host and guest, thus reducing CP transfer. The ^{13}C peaks of the PFBA guest in Figure 11 are broader for 2:1 and narrower for 1:1, and this suggests that guest dynamics are faster in the 1:1 complex. In general, differences in line shapes and δ values observed in the $^{19}\text{F} \rightarrow ^{13}\text{C}$ CP/MAS NMR results reveal differences in the guest geometry, mobility, and solvent effect in these complexes and are in agreement with the DSC, FT-IR, and ^{19}F NMR results.

3.9. Relaxation Dynamics Data. The dynamics of the guest in the complexes were studied using ^{19}F relaxation (T_1/T_2) NMR methods at variable temperature (VT; 20–70 °C). The T_1/T_2 data as a function of temperature are shown in Figure 12a–d for the 1:1 and 2:1 complexes. The T_1 process of the 1:1 complex (Figure 12a) shows a biexponential behavior as a function of temperature, whereas the 2:1 preparation (Figure 12c) shows relatively linear behavior. The biexponential behavior of the 1:1 preparation suggests that this material consists of two contributions and may be consistent with the presence of equimolar amounts of 1:1 and 2:1 host/guest complexes as illustrated by the ^{19}F NMR deconvolutions of the CF_3 peaks in Figure 9a. In contrast, the linear behavior of the 2:1 preparation is consistent with the presence of the 2:1 complex as the predominant product in this material. It should be noted here that the biexponential behavior of the 1:1 complex could be the result of multiple dynamic processes at work.

The relaxation of spin-1/2 (e.g., ^{19}F) nuclei results from fluctuations in local fields arising from chemical shift anisotropy (CSA) and dipole–dipole (DD) coupling interactions modulated by localized motions.⁵⁸ The faster the rate of motion, the less efficient the CSA and DD relaxation mechanisms and the longer the T_1/T_2 relaxation times. Notice from Figure 12 that the T_1 relaxation times increase monotonically with temperature, and this suggests that the motions that give rise to T_1 are faster than the Larmor frequency (469 MHz) at the measured conditions. However, the T_2 values (~ 0.2 – 1.3 ms) are about 3

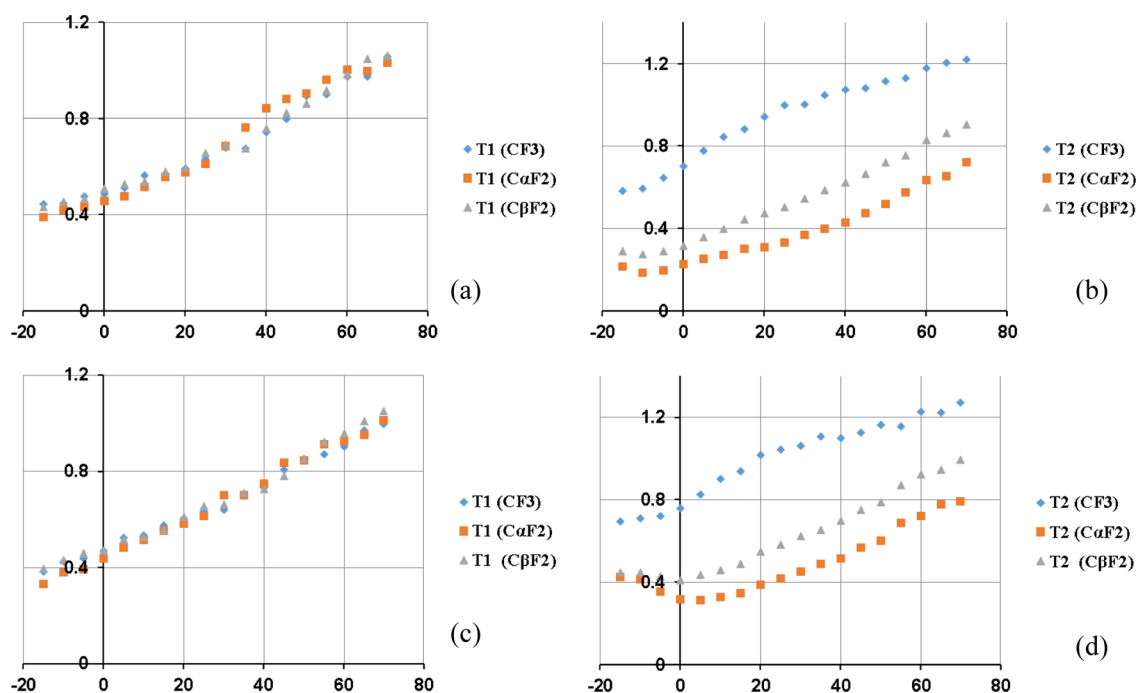


Figure 12. ^{19}F T_1 (in seconds) and T_2 (in milliseconds) relaxation times for the (a,b) 1:1 and (c,d) 2:1 β -CD/PFBA complexes.

Table 3. T_1 and T_2 Relaxation Values for the 1:1 β -CD/PFBA and 1:1 β -CD/PFOA Complexes

T ($^{\circ}\text{C}$)	1:1 β -CD/PFBA				1:1 β -CD/PFOA			
	T_1 (s)		T_2 (ms)		T_1 (s)		T_2 (ms)	
	CF_3	CF_3	$\text{CF}_2\alpha$	$\text{CF}_2\beta$	CF_3	CF_3	CF_2m	CF_2t
0	0.487	0.704	0.226	0.318	0.926	0.402	0.281	0.405
10	0.563	0.844	0.272	0.400	0.941	0.422	0.31	0.400
20	0.593	0.943	0.311	0.474	0.960	0.443	0.339	0.431
30	0.679	1.002	0.368	0.543	1.058	0.473	0.358	0.499
40	0.742	1.072	0.430	0.624	1.024	0.491	0.372	0.512
50	0.895	1.116	0.517	0.723	1.074	0.514	0.358	0.562
55	0.901	1.126	0.574	0.754	1.080	0.516	0.360	0.572
60	0.976	1.179	0.636	0.828	1.168	0.528	0.369	0.558
65	0.975	1.203	0.652	0.862	1.193	0.531	0.350	0.577
70	1.059	1.218	0.720	0.903	1.123	0.540	0.355	0.617

orders of magnitude smaller than the corresponding T_1 values (~ 0.4 – 1.0 s, cf. Table 3). This implies that the types of motion causing T_1 and T_2 relaxation are different. Starting with T_1 from Figure 12a,c, we observe that the T_1 relaxation values for the different segments of the chain at each temperature are indistinguishable in both the 1:1 (Figure 12a) and 2:1 (Figure 12c) complexes. This suggests that the type of motion that drives T_1 relaxation affects different segments of the chain similarly. That motion must be a librational (axial) motion of the guest as a whole. In contrast to the T_1 values, the T_2 values (Figure 12b,d) are different for the different segments of the chain at each temperature. We therefore conclude that the internal rotation of the CF_3 is causing T_2 relaxation, where the group furthest removed from the CF_3 group (i.e., $\text{C}_\alpha\text{F}_2$) experiences the most attenuated relaxation time because of less efficient spin diffusion.⁵⁴

In general, the T_2 values of the CF_3 group for the complexes reported herein are about twice as long compared to similar values reported previously for β -CD/PFOA complexes (cf. Table 3). This is because the motional dynamics of the short PFBA chain are expected to be significantly faster compared to

the dynamics of PFOA. Furthermore, it is evident from Figure 12b,d that the T_2 relaxation values of the methylene groups of PFBA are significantly reduced relative to those of the CF_3 group. In a previous study of β -CD/PFOA complexes,¹⁹ the T_2 values of the methylene (main and terminal) groups were close to the corresponding T_2 values of the CF_3 group as shown in Figure SI-1 of Supporting Information. Because T_2 relaxation is driven by CF_3 rotation, the reduced relaxation times for the methylene groups of the complexes reported herein further support the relative dynamics of the main PFBA chain, as described in the ^{19}F NMR simulation results in solution. The PFBA chain was described to experience extensive rotation of the CF_3 group at the termini and appreciable rotation of the CF_2 bonds in the main chain. Thus, spin diffusion propagates the CF_3 rotational motion along the chain less efficiently, resulting in reduced T_2 relaxation values for the CF_2 groups of PFBA. The increased disparity between the T_2 values of the methyl and methylene groups in the 1:1 complex compared to the 2:1 complex in Figure 12b,d may be related to the increased rotation of the CF_3 group in the former complex in accordance with the configurations in Scheme 3.

The activation energies for the methyl and methylene groups were estimated from the slope of the Arrhenius plots to further evaluate the structure of the β -CD/PFBA complexes. The results are presented in Table 4. Note that the energies of

Table 4. Activation Energies (Kilojoules per Mole) of PFBA Guest as Estimated from T_1/T_2 Data of β -CD/PFBA Complexes

	parameter	CF ₃	C _{α} F ₂	C _{β} F ₂
β -CD/PFBA 1:1	T_1	7.83	9.33	8.06
	T_2	4.12	14.4	11.1
β -CD/PFBA 2:1	T_1	8.26	9.21	8.45
	T_2	3.56	12.6	10.3

activation (E_a) for the T_1 processes are similar for all the segments (CF₃, C _{α} F₂, and C _{β} F₂) of the chain in both the 1:1 and 2:1 complexes. This supports the fact that the type of motion that drives T_1 relaxation is libration of the whole body and affects all the fluorines in the same way. Recall that T_2 is caused by the free rotation of the CF₃ group, which affects segments of the guest in different ways. This is manifested by the disparity in E_a values for the T_2 relaxation between the methyl and methylene groups (cf. Table 4).

The CF₃ groups displayed low $E_a(T_2)$ values (~ 4.0 kJ/mol), while much greater values (~ 10 – 14 kJ/mol) were recorded for the CF₂ groups. The lower $E_a(T_2)$ values for the CF₃ groups are understood in terms of the relative ease with which this group can freely rotate around its 3-fold axis. In contrast, the rotation of the CF₂–CF₂ bonds is relatively constrained in the complexes compared to that of the pure PFBA. The greater $E_a(T_1)$ for the 2:1 complex relative to the 1:1 complex suggests that the libration of the PFBA guest is more hindered in the 2:1 complex.

4. CONCLUSIONS

β -CD/PFBA host/guest inclusion compounds were prepared and characterized using multinuclear solid and solution NMR techniques, FT-IR spectroscopy, DSC, and PXRD. The solid phase compounds were prepared using a modified dissolution method at various host/guest mole ratios (1:1 and 2:1). The $^{19}\text{F} \rightarrow ^{13}\text{C}$ CP results provided unequivocal evidence for the formation of β -CD/PFBA inclusion compounds. PXRD results have shown the host to form “cage-type” structures with the guest. The enthalpy of dehydration revealed various binding configurations of the guest in the 1:1 and 2:1 complexes. According to the deconvolution analyses of the ^{19}F resonance line shapes, the guest molecule in the 1:1 preparation exists in at least two distinct configurations that resemble an equimolar mixture of 1:1 and 2:1 complexes and are supported by DSC results. In the 2:1 preparation, the contribution of the guest configuration corresponding to the 2:1 complex is predominant. The guest molecule in the 1:1 complex adopts a *gauche* conformation and is different from the fully linear conformation of the guest in the 2:1 complex. Simulation of the ^{19}F spectrum of pure PFBA and its complexes with β -CD in solution reveal that the CF₃ group experiences an extensive rotation about its 3-fold axis, whereas a significant rotation of the CF₂ is present in the main chain. NMR relaxation dynamic parameters reveal that these dynamics depend on the host/guest mole ratios and are determined by the geometry of the guest within the host. The CF₂ bond rotations are more hindered in the 2:1 complex because of full encapsulation of the guest in this product.

■ ASSOCIATED CONTENT

Supporting Information

Plots of ^{19}F T_1 and T_2 relaxation times for the 1:1 and 2:1 β -CD/PFOA complexes at variable temperature (Figure SI-1) and deconvolution parameters for the CF₃ and the CF₂ high- and low-field resonance lines of ^{19}F spectrum of the 1:1 and 2:1 β -CD/PFBA complexes acquired at MAS 20 kHz and 295 K (Tables SI-1a and SI-1b, respectively). This material is available free of charge via the Internet at <http://pubs.acs.org>.

■ AUTHOR INFORMATION

Notes

The authors declare no competing financial interest.

■ ACKNOWLEDGMENTS

We acknowledge the University of Saskatchewan, the University of Lethbridge, and the National Sciences and Engineering Council (NSERC) for supporting this research.

■ REFERENCES

- (1) Kissa, E. *Fluorinated Surfactants and Repellents*, 2nd ed.; Marcel Dekker, Inc.: New York, 2001; Vol. 97, pp 228–231.
- (2) *Organofluorine Chemistry Principles and Commercial Applications*. Banks, R. E.; Smart, B. E.; Tatlow, J. C., Eds.; Plenum Press: New York, 1994; p 61.
- (3) Erkoc, S.; Erkoc, F. Structural and electronic Properties of PFOS and LiPFOS. *J. Mol. Struct.: THEOCHEM* **2001**, *549*, 289–293.
- (4) Schultz, M. M.; Barofsky, D. F.; Field, J. A. Fluorinated Alkyl Surfactants. *Environ. Eng. Sci.* **2003**, *20*, 487–501.
- (5) Ellis, D. A.; Denkenberger, K. A.; Burrow, T. E.; Mabury, S. A. The Use of ^{19}F NMR to Interpret the Structural Properties of Perfluorocarboxylate Acids: A Possible Correlation with Their Environmental Disposition. *J. Phys. Chem. A* **2004**, *108*, 10099–10106.
- (6) Ahrens, L.; Taniyasu, S.; Yeung, L. W. Y.; Yamashita, N.; Lam, P. K. S.; Ebinghaus, R. Distribution of Polyfluoroalkyl Compounds in Water, Suspended Particulate Matter and Sediment from Tokyo Bay, Japan. *Chemosphere* **2010**, *79*, 266–272.
- (7) Giesy, J. P.; Kannan, K. Aquatic Toxicology of Perfluorinated Chemicals. *Environ. Sci. Technol.* **2001**, *35*, 1339–1342.
- (8) Prevedouros, K.; Cousins, I. T.; Buck, R. C.; Korzeniowski, S. H. Sources, Fate, and Transport of Perfluorocarboxylates. *Environ. Sci. Technol.* **2006**, *40*, 32–44.
- (9) Huset, C. A. Determination of Fluorochemicals in Waste-Dominated Aqueous Systems. Ph.D. Thesis, Oregon State University, Corvallis, OR, 2007.
- (10) Huset, C. A.; Barlaz, M. A.; Barofsky, D. F.; Field, J. A. Quantitative Determination of Fluorochemicals in Municipal Landfill Leachates. *Chemosphere* **2011**, *82*, 1380–1386.
- (11) Higgins, C. P.; Luthy, R. G. Sorption of Perfluorinated Surfactants on Sediments. *Environ. Sci. Technol.* **2006**, *40*, 7251–7256.
- (12) Karoyo, A. H.; Borisov, A. S.; Wilson, L. D.; Hazendonk, P. Formation of the Host-Guest Complexes of β -Cyclodextrin and Perfluorooctanoic Acid. *J. Phys. Chem. B* **2011**, *115*, 9511–9527.
- (13) Karoyo, A. H. Structural Studies of Supramolecular Host-Guest Systems. Ph.D. Thesis, University of Saskatchewan, Saskatoon, Canada, 2014; Chapter 5.
- (14) Szejtli, J. Introduction and General Overview of Cyclodextrin Chemistry. *J. Mater. Chem.* **1997**, *7*, 575–587.
- (15) Moroi, Y.; Yano, H.; Shibata, O.; Yonemitsu, T. Determination of Acidity Constants of Perfluoroalkanoic Acids. *Bull. Chem. Soc. Jpn.* **2001**, *74*, 667–672.
- (16) Rayne, S.; Forest, K. Theoretical Studies on the pK_a Values of Perfluoroalkyl Carboxylic Acids. *J. Mol. Struct.: THEOCHEM* **2010**, *949*, 60–69.
- (17) Bunn, C. W.; Holmes, D. R. Chain Configurations in Crystals of Linear Polymers. *Discuss. Faraday Soc.* **1958**, *25*, 95–103.

- (18) Milne, J. B.; Parker, T. J. Dissociation-Constant of Aqueous Trifluoroacetic-Acid by Cryoscopy and Conductivity. *J. Solution Chem.* **1981**, *10*, 479–487.
- (19) Karoyo, A. H.; Sidhu, P.; Wilson, L. D.; Hazendonk, P. Characterization and Dynamic Properties for the Solid Inclusion Complexes of β -Cyclodextrin and Perfluorooctanoic Acid. *J. Phys. Chem. B* **2013**, *117*, 8269–8282.
- (20) Emerging Contaminants – Perfluorooctane Sulfonate (PFOS) and Perfluorooctanoic Acid (PFOA); EPA 505-F-14-001; U.S. Environmental Protection Agency, May 2012.
- (21) Margot, R.; Berger, U.; Broman, D.; Cousins, I. R.; Nilsson, E. D.; McLachlan, M. S. Water-to-air Transfer of Perfluorinated Carboxylates and Sulfonates in a Sea Spray Simulator. *Environ. Chem.* **2001**, *8*, 381–388.
- (22) Yoo, H.; Guruge, K. S.; Yamanaka, N.; Sato, C.; Mikami, O.; Miyazaki, S.; Yamashita, N.; Giesy, J. P. Depuration Kinetics and Tissue Disposition of PFOA and PFOS in White Leghorn Chickens (*Gallus gallus*) Administered by Subcutaneous Implantation. *Ecotoxicol. Environ. Saf.* **2007**, *72*, 26–36.
- (23) Beare-Rogers, J.; Dieffenbacher, A.; Holm, J. V. Lexicon of Lipid Nutrition. *Pure Appl. Chem.* **2001**, *73*, 685–744.
- (24) Hoffmann, H.; Würtz, J. Unusual Phenomena in Perfluorosurfactants. *J. Mol. Liq.* **1997**, *72*, 191–230.
- (25) Bennett, A. E.; Rienstra, C. M.; Auger, M.; Lakshmi, K. V.; Griffin, R. G. Heteronuclear Decoupling in Rotating Solids. *J. Chem. Phys.* **1995**, *103*, 6951–6958.
- (26) Riga, A.; Collins, R.; Mlachak, G. Oxidative Behavior of Polymers by Thermogravimetric Analysis, Differential Thermal Analysis and Pressure Differential Scanning Calorimetry. *Thermochim. Acta* **1998**, *324*, 135–149.
- (27) Yang, X.; Zhao, Y.; Chen, Y.; Liao, X.; Gao, C.; Xiao, D.; Qin, Q.; Yi, D.; Yang, B. Host-Guest Inclusion System of Mangiferin with β -Cyclodextrin and its Derivatives. *Mater. Sci. Eng., C* **2013**, *33*, 2386–2391.
- (28) Cwiertnia, B.; Hladon, T.; Stobiecki, M. Stability of Dichlofenac Sodium in the Inclusion Complex with β -Cyclodextrin in the Solid State. *J. Pharm. Pharmacol.* **1999**, *51*, 1213–1218.
- (29) Venkatesh, G.; Sivasankar, T.; Karthick, M.; Rajendiraan, N. Inclusion Complexes of Sulphanilamide Drugs and β -Cyclodextrin: A Theoretical Approach. *J. Inclusion Phenom. Macrocyclic Chem.* **2013**, *77*, 309–318.
- (30) Palepu, R.; Reinsborough, V. C. Surfactant Cyclodextrin Interactions by Conductance Measurements. *Can. J. Chem.* **1988**, *66* (2), 325–328.
- (31) Wenz, G. Cyclodextrins as Building Blocks for Supramolecular Structures and Functional Units. *Angew. Chem., Int. Ed. Engl.* **1994**, *33*, 803–822.
- (32) Wilson, L. D.; Verrall, R. E. ^{19}F and ^1H NMR Investigation of Cyclodextrin/Fluorocarbon Alkyl Carboxylate Surfactant Inclusion Complexes. *Langmuir* **1998**, *14*, 4710–4717.
- (33) Dong, T.; He, Y.; Shin, K.; Inoue, Y. Formation and Characterization of Inclusion Complexes of Poly(butylene succinate) with α - and γ -Cyclodextrins. *Macromol. Biosci.* **2004**, *4* (12), 1084–1091.
- (34) Lamcharfi, E.; Kunesch, G.; Meyer, C.; Robert, B. Investigation of Cyclodextrin Inclusion Compounds using FT-IR and Raman Spectroscopy. *Spectrochim. Acta, Part A* **1995**, *51*, 1861–1870.
- (35) Harry-O'kuru, R. E.; Isbell, T. A.; Weisleder, D. Synthesis of Estolide Esters from cis-9-octadecenoic Acid Estelides. *J. Am. Oil Chem. Soc.* **2001**, *71*, 219–222.
- (36) Labuschagne, P. W.; Kazarian, S. G.; Sadiku, R. E. *In Situ* FT-IR Spectroscopic Study of the Effect of CO_2 Sorption on H-bonding in PEG-PVP Mixtures. *Spectrochim. Acta, Part A* **2011**, *78*, 1500–1506.
- (37) Moynihan, R. E. The Molecular Structure of Perfluorocarbon Polymers. Infrared Studies on Polytetrafluoroethylene. *J. Am. Chem. Soc.* **1959**, *81*, 1045–1050.
- (38) Wang, J.; Ober, C. K. Solid State Crystalline and Liquid Crystalline Structure of Semifluorinated 1-Bromoalkane Compounds. *Liq. Cryst.* **1999**, *26*, 637–648.
- (39) Knonchehuer, G.; Reiche, J.; Brehmwer, L.; Berberka, T.; Woolley, M.; Tredgold, R.; Hodge, P. J. Do Perfluorinated Chains Always Have to be Twisted? *Chem. Soc., Chem. Commun.* **1995**, 1619–1620.
- (40) Albinsson, B.; Michl, J. Anti, Ortho, and Gauche Conformers of Perfluoro-*n*-butane: Matrix-Isolation IR Spectra and Calculations. *J. Phys. Chem.* **1996**, *100*, 3418–3429.
- (41) Okumura, H.; Kawaguchi, Y.; Harada, A. Preparation and Characterization of Inclusion Complexes of Poly(dimethylsiloxane)s with Cyclodextrins. *Macromolecules* **2001**, *34*, 6338–6343.
- (42) Schneider, H.-J.; Hacket, F.; Rüdiger, V. NMR Studies of Cyclodextrins and Cyclodextrin Complexes. *Chem. Rev. (Washington, DC, U.S.)* **1998**, *98*, 1755–1785.
- (43) Steed, J. W.; Atwood, J. L. In *Supramolecular Chemistry*, 2nd ed.; John Wiley & Sons, Ltd.: West Sussex, UK, 2009.
- (44) Guo, W.; Fung, B. M.; Christian, S. D. NMR Study of Cyclodextrin Inclusion of Fluorocarbon Surfactants in Solution. *Langmuir* **1992**, *8*, 446–451.
- (45) Yonemori, S.; Sasakura, H. Structural Determination of Fluoro-Organic Mixtures by ^{19}F COSY NMR Spectroscopy. *J. Fluorine Chem.* **1995**, *75*, 151–156.
- (46) Emsley, J. W.; Feeney, J.; Sutcliffe, L. J. *High-Resolution Magnetic Resonance Spectroscopy*. Pergamon: New York, 1966; Vol. 2, p 877.
- (47) Newmark, R. A. Vicinal Fluorine-Fluorine Coupling Constants in Perfluoropropyl Groups. *J. Fluorine Chem.* **2009**, *130*, 383–393.
- (48) Foris, A. ^{13}C NMR Spectra of Halocarbons. *Magn. Reson. Chem.* **2001**, *39*, 386–398.
- (49) Gutowsky, H. S.; Belford, G. G.; McMahon, P. E. NMR Studies of Conformational Equilibria in Substituted Ethanes. *J. Chem. Phys.* **1962**, *36*, 3353–3368.
- (50) Borisov, A. S.; Hazendonk, P.; Hayes, P. G. ^{31}P MAS NMR Spectroscopy of Hexachlorocyclotriphosphazene at Different Stages During Thermal Ring-Opening Polymerization. *J. Inorg. Organomet. Polym.* **2008**, *18*, 163–174.
- (51) Koito, Y.; Yamada, K.; Ando, S. Solid-state NMR and Wide-angle X-ray Diffraction Study of Hydrofluoroether/ β -Cyclodextrin Inclusion Complex. *J. Inclusion Phenom. Macrocyclic Chem.* **2013**, *76*, 143–150.
- (52) Fyfe, C. A.; Brouwer, D. H. Determination of the Location of Naphthalene in the Zeolite ZSM-5 Host Framework by Solid-state $^1\text{H}/^{29}\text{Si}$ CP MAS NMR Spectroscopy. *Can. J. Chem.* **2006**, *84*, 345–355.
- (53) Lefebvre, F.; Mentzen, B. F. Study of Sorbent-Sorbate Interactions in Some Aromatics Silicalite Systems by Use of Nuclear Magnetic Resonance with Cross-Polarization. *Mater. Res. Bull.* **1994**, *29*, 1049–1056.
- (54) Derome, A. E. In *Modern NMR Techniques for Chemistry*; Pergamon: New York, 1987.
- (55) Jiao, H.; Goh, S. H.; Valiyaveetil, S. Inclusion Complexes of Poly(4-vinylpyridine)-Dodecylbenzenesulfonic Acid Complex and Cyclodextrins. *Macromolecules* **2002**, *35*, 3997–4002.
- (56) Balci, M. *Basic ^1H - and ^{13}C -NMR Spectroscopy*. 1st ed. Elsevier B. V.: Amsterdam, The Netherlands, 2005; chp 13, pp 315–319.
- (57) Lim, K. T.; Ganapathy, H. S.; Lee, M. Y.; Yuvaraj, H.; L, W.-K.; Heo, H. A Facile One-pot Synthesis of Novel Amphiphilic Perfluoroalkyl Ester Functionalized γ -Cyclodextrin and Complex Formation with Anionic Surfactants. *J. Fluorine Chem.* **2006**, *127*, 730–735.
- (58) Levitt, M. L. *Spin Dynamics: Basics of Nuclear Magnetic Resonance*, 2nd ed.; John Wiley & Sons Ltd: Chichester, U.K., 2005.